Fast algorithm for quadratic aberration model in optical lithography based on cross triple correlation

Shiyuan Liu
Huazhong University of Science and Technology
Wuhan National Laboratory for Optoelectronics
1037 Luoyu Road
Wuhan 430074, China
and
Huazhong University of Science and Technology
State Key Laboratory of Digital Manufacturing Equipment and Technology
Wuhan 430074, China
E-mail: shyliu@mail.hust.edu.cn

Wei Liu
Huazhong University of Science and Technology
Wuhan National Laboratory for Optoelectronics
Wuhan 430074, China

Tingting Zhou
Huazhong University of Science and Technology
State Key Laboratory of Digital Manufacturing Equipment and Technology
Wuhan 430074, China

Abstract. The quadratic aberration model used in optical lithography is a natural extension of the linear model by taking into account interactions among individual Zernike coefficients. Although the model has been tested and verified in many applications, the effects of Zernike coefficients under partially coherent imaging are usually obtained by extensive experiments due to the complexity of the model expression. In this paper, a generalized cross triple correlation (CTC) is introduced and a fast algorithm to simulate the quadratic aberration model is developed. Simulations were performed by the proposed CTC-based algorithm with different input Zernike aberrations for binary and phase shift masks with multiple pitches and orientations, which demonstrate that the proposed approach is not only accurate but also efficient for revealing the influence of different Zernike orders on aerial image intensity distributions under partially coherent illumination. [DOI: 10.1117/1.3586797]

Subject terms: wavefront aberration; quadratic aberration model; cross triple correlation; transmission cross coefficient; partial coherent imaging; optical lithography.

Paper 11010PR received Jan. 27, 2011; revised manuscript received Apr. 4, 2011; accepted for publication Apr. 12, 2011; published online May 16, 2011.

1 Introduction

As the limit of optical lithography is pushed and feature densities continue to increase, lens aberration has become one of the most important factors to evaluate the imaging quality of lithographic tools.[1–3] One method to mathematically model lens aberrations utilizes Zernike polynomials, which are a complete orthogonal set of polynomials over the interior of the unit circle.[4,5] The Zernike series representation is useful as it provides explicit expressions for the well-known aberrations such as spherical, coma, astigmatism, etc., which can be classified into odd and even aberrations. Odd aberrations cause image displacement and line-width asymmetry that influence critical dimension uniformity,[6] together with even aberrations reducing the maximum image irradiance and image log-slope, which affects the usable depth of focus.[7] Moreover, the interaction among different types of aberrations brings about the distinct deterioration of intensity or relative parameters such as critical dimension (CD) uniformity and position shift.[8] Considering the multiplicity of the Zernike aberration in practical projection lens, a detailed understanding and evaluation of the effects of wavefront aberration represented by Zernike coefficients on imaging is crucial in lithography.

The imaging optics configuration in lithographic tools is typically a partially coherent system that is characterized by the intensity distribution of the effective source and the pupil function of the projection lens. Imaging properties of such partially coherent systems have to be described using a bilinear model,[9] which leads to time-consuming calculations and difficulties in comprehension, especially in the case when the wavefront aberration is involved. In recent years, an approximate linear response model of Zernike coefficients to the aerial image displacement has been reported and widely utilized for aberration comprehension and measurement. The linear relationship can be established between the intensity difference of adjacent peaks in the one-dimensional binary gating images,[6,7,10] by supposing that the individual Zernike aberration in the current lithographic projection lens is very small. Although this linear response model has a wide real-world application of Zernike aberration characterization based on one-dimensional masks, it is necessary to develop a more generalized Zernike response model suitable not only for one-dimensional but also for two-dimensional masks with a relatively large amount of individual Zernike aberration. A quadratic aberration model that is a natural extension of the linear response model has been reported by taking into account interactions among individual Zernike aberrations.[11] The quadratic aberration model has been tested and verified in many applications under both one-dimensional and two-dimensional masks, such as CD uniformity,[8] aberration sensitivity analysis,[12] through-focus imaging modeling,[13] and aberration monitoring using phase wheel targets.[14] However, the effects of Zernike aberrations on partially coherent imaging are usually obtained through extensive experiments or by the use of lithographic simulators,[15] due to the complexity of the model formulation. The calculation of the quadratic aberration model directly by analytical expression is time consuming and thus impractical for *in-situ* measurement or characterization.

In this paper, a generalized cross triple correlation (CTC) is introduced for rapidly calculating the quadratic

1932-5150/2011/$25.00 © 2011 SPIE

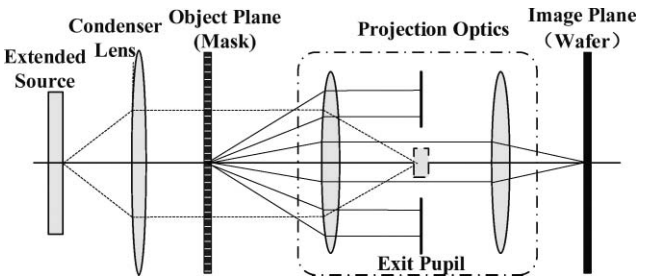

Fig. 1 Optical lithography imaging system.

aberration model. By decomposition of the transmission cross coefficient (TCC) into CTCs, the Zernike aberration-induced intensities in the quadratic aberration model can be quickly calculated and clearly separated from each other. Simulations were performed by the proposed CTC-based algorithm with different input Zernike aberrations for binary and phase shift masks with multiple pitches and orientations, which demonstrates that the proposed approach is not only accurate but also efficient for revealing the influence of different Zernike orders on aerial image intensity distributions under partially coherent illumination. It is expected that this method will have direct applications in the aerial image-based aberration analysis and metrology. It will also have potential applications in the robust optical proximity correction (OPC) and inverse mask design with aberrations taken into account.

2 Theory

2.1 *Optical Imaging System*

An optical lithography imaging system is shown in Fig. 1, in which both the object and the light source are of finite extent. In order to simplify the expressions of the imaging system, in the drawing we introduce the Cartesian object plane coordinates $\mathbf{x_0}$, image plane coordinates $\mathbf{x}$ and pupil plane coordinates $\mathbf{f}$, which are two-dimensional real vectors and all normalized according to canonical coordinates proposed by Hopkins;[2] thus the cut-off frequency from the pupil plane is normalized to the unit of one. The scalar form of Hopkins imaging theory for partially coherent imaging is used to depict its behavior[16]

$$I(\mathbf{x}) = \iint O(\mathbf{f}_1)O^*(\mathbf{f}_2)\mathrm{TCC}(\mathbf{f}_1,\mathbf{f}_2) \times \exp[-2\pi i(\mathbf{f}_1-\mathbf{f}_2).\mathbf{x}]d\mathbf{f}_1 d\mathbf{f}_2, \quad (1)$$

where $\mathrm{TCC}(\mathbf{f}_1,\mathbf{f}_2)$ is introduced as the concept of the transmission cross coefficient

$$\mathrm{TCC}(\mathbf{f}_1,\mathbf{f}_2) = \int J(\mathbf{f})H(\mathbf{f}+\mathbf{f}_1)H^*(\mathbf{f}+\mathbf{f}_2)d\mathbf{f}. \quad (2)$$

Here $O(\mathbf{f})$ is the diffraction spectrum of a mask pattern. $J(\mathbf{f})$ describes the effective source intensity distribution under Kohler illumination. With a conventional circular illumination, it is constant within a radius proportional to partial coherence factor σ

$$J(\mathbf{f}) = \frac{1}{\pi\sigma^2}\mathrm{circ}\left(\frac{|\mathbf{f}|}{\sigma}\right). \quad (3)$$

$H(\mathbf{f})$ is the objective pupil function and is given by

$$H(\mathbf{f}) = P(\mathbf{f})\exp[-ikW_{\mathrm{lens}}(\mathbf{f})], \quad (4)$$

where $k = 2\pi/\lambda$ is the wavenumber, λ is the wavelength of the monochromatic light source, and $W_{\mathrm{lens}}(\mathbf{f})$ indicates the lens aberration, which can be expressed as orthonormal Zernike fringe polynomials[17]

$$W_{\mathrm{lens}}(\mathbf{f}) = \sum_n Z_n R_n(\mathbf{f}), \quad (5)$$

where n indicates Zernike index, $R_n(\mathbf{f})$ indicates the nth Zernike polynomial for normalized Cartesian coordinate over the pupil plane. $P(\mathbf{f})$ is the defocused pupil function without lens aberration, and represented by

$$P(\mathbf{f}) = \mathrm{circ}(|\mathbf{f}|)\exp[-ikW_{\mathrm{defocus}}(\mathbf{f})]. \quad (6)$$

Here, an even-type aberration $W_{\mathrm{defocus}}(\mathbf{f})$ is induced by a defocus h (in nm) of the image plane

$$W_{\mathrm{defocus}}(\mathbf{f}) = h\cdot w_{\mathrm{defocus}}(\mathbf{f}) = h\left[\sqrt{1-NA^2|\mathbf{f}|^2}-1\right], \quad (7)$$

where NA is the image-side numerical aperture of the projection lens.

2.2 *Theory and Algorithm of Cross Triple Correlation*

The cross triple correlation (CTC) is defined as[18]

$$\mathrm{CTC}(\mathbf{f}_1,\mathbf{f}_2) = \int a(\mathbf{f})b(\mathbf{f}+\mathbf{f}_1)c(\mathbf{f}+\mathbf{f}_2)d\mathbf{f}, \quad (8)$$

where $a(\mathbf{f})$, $b(\mathbf{f})$, and $c(\mathbf{f})$ are three different functions. $\mathbf{f}$, $\mathbf{f}_1$, and $\mathbf{f}_2$ are variables that can be any real scalars for a one-dimensional signal or two-dimensional real vectors representing the normalized spatial-frequency pupil coordinates. Most of the physical functions required for analysis of lithographic systems have compact support, and integration can be treated over the whole space of $\mathbf{f}$. It is interesting to note that the expression of TCC in Eq. (2) is quite similar to the CTC in Eq. (8), except with the difference that the last two functions involved in TCC are two conjugate pupils instead of the two fully independent functions in CTC. Therefore, TCC can be considered as a special case of CTC.

To show the mathematical meaning of CTC, the variables $\mathbf{f}$, $\mathbf{f}_1$, and $\mathbf{f}_2$ can be simply supposed to be one-dimensional, hence, they can be indicated by f, f_1, and f_2, respectively. As shown in Fig. 2, the CTC thus becomes a two-dimensional distribution CTC (f_1, f_2), which is the integral of the product of three one-dimensional functions $a(f)$, $b(f + f_1)$, and $c(f + f_2)$ at a specific point (f_1, f_2) along the f axis. In the case that $\mathbf{f}$, $\mathbf{f}_1$, and $\mathbf{f}_2$ are two-dimensional real vectors, the CTC $(\mathbf{f}_1,\mathbf{f}_2)$ becomes a four-dimensional matrix. It is, therefore, time consuming to directly obtain each point in the four-dimensional matrix by Eq. (8), because repeating integrations are needed for different positions $(\mathbf{f}_1,\mathbf{f}_2)$ in four-dimensional Cartesian coordinates.

Köhle recently reported a fast TCC algorithm using a fast Fourier transform (FFT)-based method.[19] The concept of generalized fast convolution was first introduced to perform an accurate and efficient operation. However, the given expression and algorithm of the introduced generalized convolution are restricted to TCC calculation only, where two conjugate pupil functions are multiplied by the effective source function. This kind of convolution is, therefore, not an exact general case for any self-defined functions, such

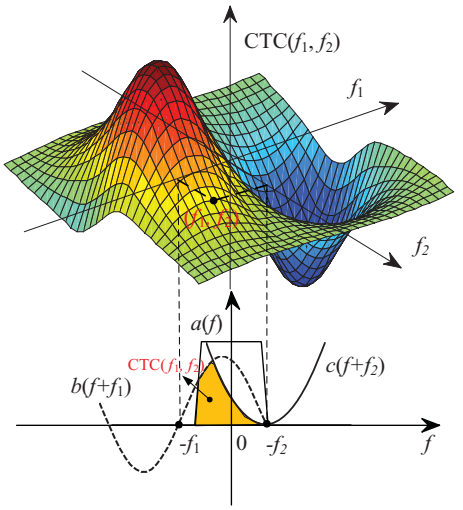

Fig. 2 Representation of the mathematical meaning of CTC.

as those three fully independent functions involved in CTC as shown in Eq. (8) and Fig. 2. Considering that TCC is a special case of CTC, in this paper we extend the generalized fast convolution from TCC to CTC and utilize an FFT-based algorithm to achieve an efficient CTC calculation.

Let ctc($\mathbf{x}_1$,$\mathbf{x}_2$), $\alpha(\mathbf{x})$, $\beta(\mathbf{x})$, and $\gamma(\mathbf{x})$ be the Fourier transforms of CTC($\mathbf{f}_1$,$\mathbf{f}_2$), $a(\mathbf{f})$, $b(\mathbf{f})$, and $c(\mathbf{f})$, respectively. Based on the theorem of Tichmarch, the CTC can be treated as a kind of more generalized convolution, and then the ctc($\mathbf{x}_1$,$\mathbf{x}_2$), $\alpha(\mathbf{x})$, $\beta(\mathbf{x})$, and $\gamma(\mathbf{x})$ satisfy[18]

$$\mathrm{ctc}(\mathbf{x}_1, \mathbf{x}_2) = \alpha(\mathbf{x}_1)\beta(\mathbf{x}_2)\gamma(-\mathbf{x}_1 - \mathbf{x}_2). \tag{9}$$

From Eq. (9), a generalized fast CTC algorithm can be developed as shown in Fig. 3. It can be noted that the FFT-based CTC algorithm takes advantage of the reported FFT-based TCC algorithm[19] but shows some obvious difference and improvement. The detailed procedure of the FFT-based CTC calculation is depicted as follows. 1. Perform FFT2 (two-dimensional FFT) to $a(\mathbf{f})$, $b(\mathbf{f})$, and $c(\mathbf{f})$ in order to obtain the corresponding two-dimensional functions $\alpha(\mathbf{x})$, $\beta(\mathbf{x})$, and $\gamma(\mathbf{x})$ in the spatial domain, as variables $\mathbf{f}$ and $\mathbf{x}$ indicate two-dimensional real vectors; 2. prepare $\alpha(\mathbf{x}_1)$, $\beta(\mathbf{x}_2)$, and $\gamma(-\mathbf{x}_1 - \mathbf{x}_2)$ for the next step, by substituting different variables $\mathbf{x} = \mathbf{x}_1$, $\mathbf{x} = \mathbf{x}_2$, and $\mathbf{x} = -\mathbf{x}_1 - \mathbf{x}_2$ into functions $\alpha(\mathbf{x})$, $\beta(\mathbf{x})$, and $\gamma(\mathbf{x})$, respectively; 3. calculate four-dimensional function ctc($\mathbf{x}_1$,$\mathbf{x}_2$) by multiplication of $\alpha(\mathbf{x}_1)$, $\beta(\mathbf{x}_2)$, and $\gamma(-\mathbf{x}_1 - \mathbf{x}_2)$; and 4. complete CTC($\mathbf{f}_1$,$\mathbf{f}_2$) calculation after performing IFFT4 (four-dimensional inverse fast Fourier transform) to ctc($\mathbf{x}_1$,$\mathbf{x}_2$). It is noted that the final function CTC($\mathbf{f}_1$,$\mathbf{f}_2$) is four-dimensional and can be efficiently obtained, which directly leads to a fast algorithm for the CTC

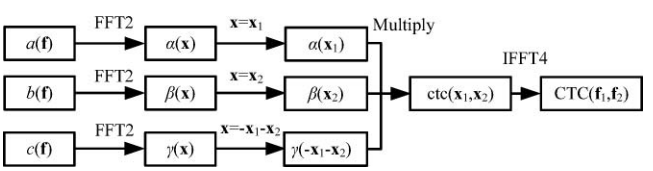

Fig. 3 Block diagram of the FFT-based CTC algorithm.

calculation as the time-consuming integration in Eq. (8) is avoided and replaced by the simple multiplication of $\alpha(\mathbf{x}_1)$, $\beta(\mathbf{x}_2)$, and $\gamma(-\mathbf{x}_1 - \mathbf{x}_2)$.

The accuracy of CTC is heavily dependent on the resolution of source function $a(\mathbf{f})$ in the simulation. So, the higher resolution the source bitmap has, the more accurate the CTC calculation results will be achieved. However, for a certain bitmap source with a high resolution in simulation, the FFT calculation of the CTC matrix at the same resolution as that of the source may exceed the memory and time constraints of most computers, because the CTC matrix becomes a huge four-dimensional matrix while the source matrix is only two-dimensional. To relax this dependency, the CTC matrix must be sampled at a lower resolution than the source. Thus, it indicates that the CTC resolution is not coupled with the source resolution. This sampling problem can be solved by polyphase decomposition methods adopted from signal processing.[19,20]

2.3 *Cross Triple Correlation-based Quadratic Aberration Model*

According to Eqs. (2) and (6), expression for TCC in the case where Zernike aberrations are induced can be written as

$$\mathrm{TCC}(\mathbf{f}_1, \mathbf{f}_2) = \int J(\mathbf{f})P(\mathbf{f}+\mathbf{f}_1)P^*(\mathbf{f}+\mathbf{f}_2) \times \exp\left\{-ik\left[\sum_n Z_n R_n(\mathbf{f}+\mathbf{f}_1) - \sum_m Z_m R_m(\mathbf{f}+\mathbf{f}_2)\right]\right\} d\mathbf{f}. \tag{10}$$

Applying the Taylor series expansion of the exponential function, the TCC in Eq. (10) can be decomposed up to quadratic terms as a TCC quadratic approximation

$$\mathrm{TCC}(\mathbf{f}_1, \mathbf{f}_2) \approx T_0(\mathbf{f}_1, \mathbf{f}_2) + T_1(\mathbf{f}_1, \mathbf{f}_2) + T_2(\mathbf{f}_1, \mathbf{f}_2), \tag{11}$$

where $T_0(\mathbf{f}_1,\mathbf{f}_2)$, $T_1(\mathbf{f}_1,\mathbf{f}_2)$, and $T_2(\mathbf{f}_1,\mathbf{f}_2)$ represent the unaberrated TCC, linearly aberrated TCC, and quadratically aberrated TCC, respectively. $T_1(\mathbf{f}_1,\mathbf{f}_2)$ and $T_2(\mathbf{f}_1,\mathbf{f}_2)$ can be further decomposed into $T_{\mathrm{lin}}^{(n)}(\mathbf{f}_1,\mathbf{f}_2)$ and $T_{\mathrm{quad}}^{(n,m)}(\mathbf{f}_1,\mathbf{f}_2)$ with a set of input Zerinke coefficients

$$\mathrm{TCC}(\mathbf{f}_1, \mathbf{f}_2) = T_0(\mathbf{f}_1, \mathbf{f}_2) + Z_n \sum_n T_{\mathrm{lin}}^{(n)}(\mathbf{f}_1, \mathbf{f}_2) + Z_n Z_m \sum_n \sum_m T_{\mathrm{quad}}^{(n,m)}(\mathbf{f}_1, \mathbf{f}_2). \tag{12}$$

Here, $T_{\mathrm{lin}}^{(n)}(\mathbf{f}_1,\mathbf{f}_2)$ and $T_{\mathrm{quad}}^{(n,m)}(\mathbf{f}_1,\mathbf{f}_2)$ are linearly aberrated TCC and quadratically aberrated TCC based on individual Zernike aberrations. Each term of $T_0(\mathbf{f}_1,\mathbf{f}_2)$, $T_{\mathrm{lin}}^{(n)}(\mathbf{f}_1,\mathbf{f}_2)$, and $T_{\mathrm{quad}}^{(n,m)}(\mathbf{f}_1,\mathbf{f}_2)$ can be represented as a weighted sum of several CTCs

$$T_0(\mathbf{f}_1, \mathbf{f}_2) = C_{0,0;0,0}(\mathbf{f}_1, \mathbf{f}_2), \tag{13}$$

$$T_{\mathrm{lin}}^{(n)}(\mathbf{f}_1, \mathbf{f}_2) = -ik[C_{n,0;0,0}(\mathbf{f}_1, \mathbf{f}_2) - C_{0,0;n,0}(\mathbf{f}_1, \mathbf{f}_2)], \tag{14}$$

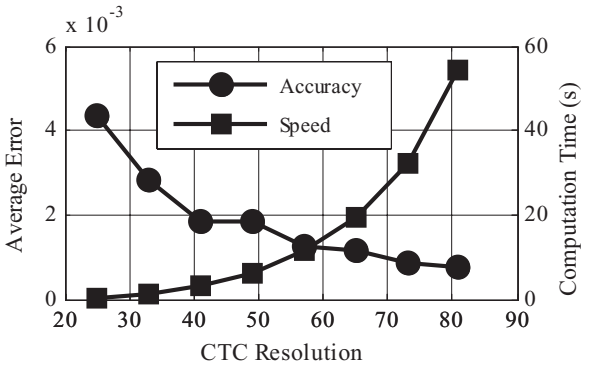

Fig. 4 Accuracy and speed of the FFT-based CTC algorithm with respect to different CTC resolutions.

$$T_{\text{quad}}^{(n,m)}(\mathbf{f}_1,\mathbf{f}_2) = -\frac{1}{2}k^2\left[C_{n,m;0,0}(\mathbf{f}_1,\mathbf{f}_2) - C_{n,0;m,0}(\mathbf{f}_1,\mathbf{f}_2) - C_{m,0;n,0}(\mathbf{f}_1,\mathbf{f}_2) + C_{0,0;n,m}(\mathbf{f}_1,\mathbf{f}_2)\right], \quad (15)$$

where $C_{k,l;m,n}(\mathbf{f}_1,\mathbf{f}_2)$ is a special CTC of the following notation with defining $R_0(\mathbf{f}) = 1$:

$$C_{k,l;m,n}(\mathbf{f}_1,\mathbf{f}_2) = \int J(\mathbf{f})\{P(\mathbf{f}+\mathbf{f}_1)[R_k(\mathbf{f}+\mathbf{f}_1)\cdot R_l(\mathbf{f}+\mathbf{f}_1)]\} \times \left\{P^*(\mathbf{f}+\mathbf{f}_2)[R_m(\mathbf{f}+\mathbf{f}_2)\cdot R_n(\mathbf{f}+\mathbf{f}_2)]\right\} d\mathbf{f}. \quad (16)$$

Consequently, substituting Eq. (12) into Eq. (1), the total image intensity can be decomposed and represented as a quadratic aberration model in the following formulation:

$$I(\mathbf{x}) \approx I_0(\mathbf{x}) + I_1(\mathbf{x}) + I_2(\mathbf{x}) = I_0(\mathbf{x}) + \sum_n Z_n I_{\text{lin}}^{(n)}(\mathbf{x}) + \sum_n \sum_m Z_n Z_m I_{\text{quad}}^{(n,m)}(\mathbf{x}), \quad (17)$$

where $I_0(\mathbf{x})$ is called the aberration-free intensity and $I_1(\mathbf{x})$ and $I_2(\mathbf{x})$ display the aberration-induced intensity distributions of linear and quadratic terms, respectively. Similar to $T_1(\mathbf{f}_1,\mathbf{f}_2)$ and $T_2(\mathbf{f}_1,\mathbf{f}_2)$, the $I_1(\mathbf{x})$ and $I_2(\mathbf{x})$ can be decomposed into $I_{\text{lin}}{}^{(n)}(\mathbf{x})$ and $I_{\text{quad}}{}^{(n,m)}(\mathbf{x})$ multiplied by the corresponding Zerinke coefficients. Thus, $I_{\text{lin}}{}^{(n)}(\mathbf{x})$ and $I_{\text{quad}}{}^{(n,m)}(\mathbf{x})$ respectively represent the linearly and quadratically aberrated aerial images based on individual Zernike aberrations. The $I_0(\mathbf{x})$, $I_{\text{lin}}{}^{(n)}(\mathbf{x})$, and $I_{\text{quad}}{}^{(n,m)}(\mathbf{x})$ can be directly calculated from $T_0(\mathbf{f}_1,\mathbf{f}_2)$, $T_{\text{lin}}{}^{(n)}(\mathbf{f}_1,\mathbf{f}_2)$, and $T_{\text{quad}}{}^{(n,m)}(\mathbf{f}_1,\mathbf{f}_2)$ by the formulations of

$$I_0(\mathbf{x}) = \iint O(\mathbf{f}_1)O^*(\mathbf{f}_2)T_o(\mathbf{f}_1,\mathbf{f}_2) \times \exp[-2\pi i(\mathbf{f}_1-\mathbf{f}_2).\mathbf{x}]d\mathbf{f}_1 d\mathbf{f}_2, \quad (18)$$

$$I_{\text{lin}}^{(n)}(\mathbf{x}) = \iint O(\mathbf{f}_1)O^*(\mathbf{f}_2)T_{lin}^{(n)}(\mathbf{f}_1,\mathbf{f}_2) \times \exp[-2\pi i(\mathbf{f}_1-\mathbf{f}_2).\mathbf{x}]d\mathbf{f}_1 d\mathbf{f}_2, \quad (19)$$

and

$$I_{\text{quad}}^{(n,m)}(\mathbf{x}) = \iint O(\mathbf{f}_1)O^*(\mathbf{f}_2)T_{quad}^{(n,m)}(\mathbf{f}_1,\mathbf{f}_2) \times \exp[-2\pi i(\mathbf{f}_1-\mathbf{f}_2).\mathbf{x}]d\mathbf{f}_1 d\mathbf{f}_2. \quad (20)$$

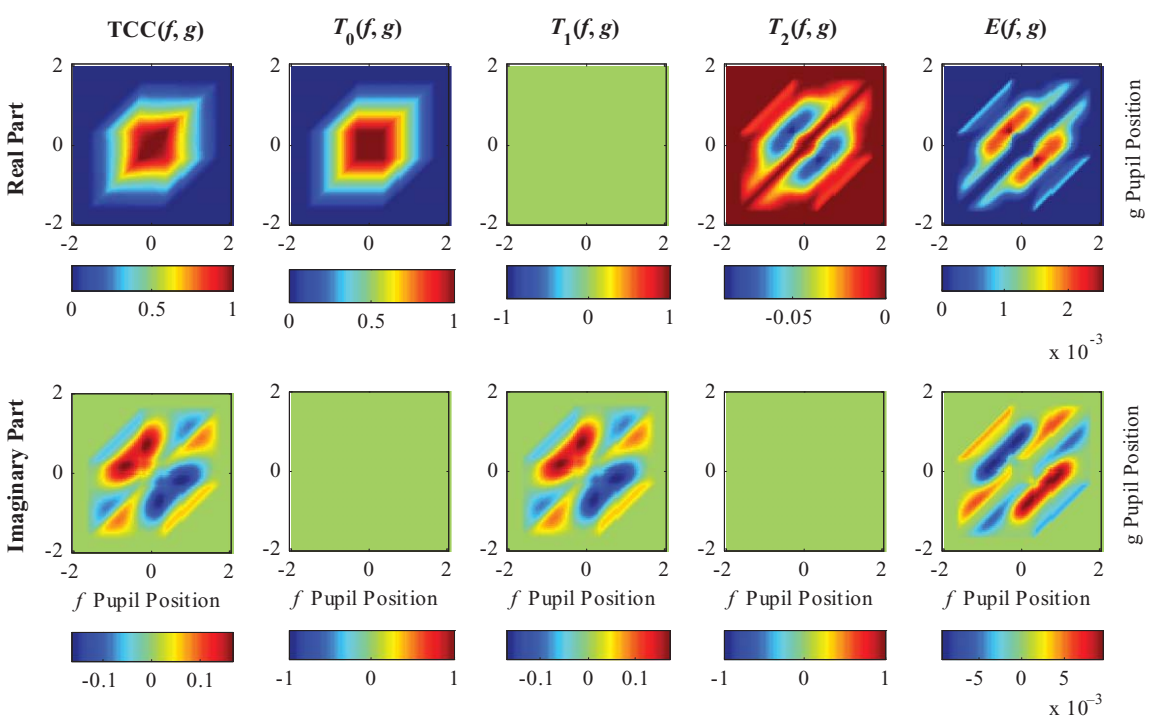

Fig. 5 Example of decomposing TCC(f, g) into the unaberrated term $T_0(f, g)$, linearly aberrated term $T_1(f, g)$, and quadratically aberrated term $T_2(f, g)$ under the input Zernike coefficient $Z_7 = 0.1\lambda$.

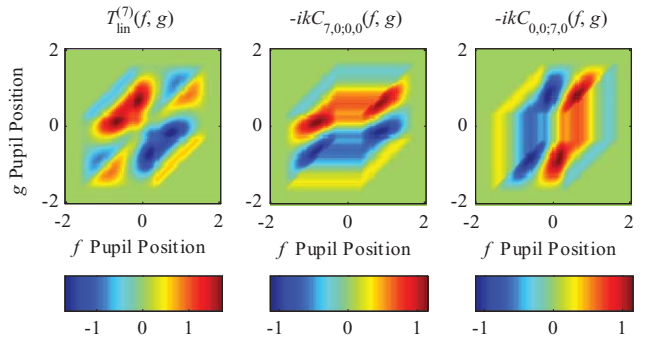

Fig. 6 Representation of the linearly aberrated TCC term $T_{lin}^{(7)}(f, g)$ as a sum of weighted CTCs.

3 Simulations

3.1 *Accuracy and Speed Estimation of the Fast Fourier Transform-based Cross Triple Correlation Algorithm*

The FFT-based CTC algorithm is a key factor for building the quadratic aberration model. To achieve a fast quadratic aberration modeling, it is important and necessary to estimate the accuracy and speed of CTC calculation.

A set of four-dimensional CTCs with multiple resolutions from 25 to 81 were operated on an HP Z600 Workstation of 2.53 GHz Opteron with MATLAB in Windows 7 (64-bit). The parameters in an optical imaging system were set as $Z_7 = 0.1\lambda$, $\lambda = 193$ nm, and NA $= 0.75$, with a partial coherence factor of 0.35 and defocus of 0 nm. The resolutions of input sources were set at three times the corresponding CTC resolutions. The calculation accuracy was evaluated by the average error between the FFT-based CTC matrix and the corresponding reference CTC matrix that was calculated by direct integration as shown in Eq. (8). The FFT-based CTC matrix and the reference CTC matrix were both normalized so that the maximum value in each of the matrix was unit one. Figure 4 illustrates the accuracy and speed of the FFT-based CTC algorithm with respect to different CTC resolutions.

From the simulation results shown in Fig. 4, it is clear that the calculation error decreases as the CTC resolution increases. In contrary, the calculation time increases when increasing the CTC resolution. The simulation results confirm that the higher the source resolution is, the more accurate the CTC calculation results can be achieved. In addition, although increasing the CTC resolution will reduce the calculation speed, based on the proposed algorithm, a four-dimensional CTC matrix with up to 81 elements[4] can be efficiently calculated in 55.5 s. It, thus, demonstrates that the FFT-based CTC algorithm provides an efficient and accurate approach to implement the quadratic aberration model shown in Eq. (17).

3.2 *Simulation of the Transmission Cross Coefficient Quadratic Approximation*

We further performed simulations on the imaging system operating at $\lambda = 193$ nm, NA $= 0.75$, and defocus $= 0$ nm, with a partial coherence factor of 0.70. The real vectors $\mathbf{f}_1$, $\mathbf{f}_2$ denote (f, f') and (g, g') in two-dimensional Cartesian coordinates, respectively. Since both CTC and TCC are represented by four-dimensional matrices in Cartesian coordinates $(\mathbf{f}_1, \mathbf{f}_2)$ or $(f, g; f', g')$, the cross sections of the corresponding CTC and TCC can be depicted by a matrix slice, which is a two-dimensional matrix in Cartesian coordinates (f, g) by considering $f' = 0$ and $g' = 0$. To guarantee that the simulation results of CTCs are more accurate, the size of the CTC matrix was chosen to be 73 (Ref. 4) with the resolution fixed to 73. Figure 5 depicts an example of decomposing TCC(f, g) into the unaberrated term $T_0(f, g)$, the linear term $T_1(f, g)$, and the quadratic term $T_2(f, g)$ under the input of an individual Zernike coefficient $Z_7 = 0.1\lambda$. The $E(f, g)$ is defined as a residual TCC calculated by $E(f, g) = \text{TCC}(f, g) - [T_0(f, g) + T_1(f, g) + T_2(f, g)]$.

From Fig. 5, it is obvious that the TCC(f, g) is a complex value due to the fact that the aberration $W(\mathbf{f})$ itself is real but its exponential function term for phase change is complex in Eq. (10). Because defocus $= 0$ nm was set in the simulation, each of the $C_{k,l;m,n}(\mathbf{f}_1,\mathbf{f}_2)$ obtained by Eq. (16) remains as a real value. Determined by Eqs. (11)–(15), the linear term $T_1(f, g)$ and quadratic term $T_2(f, g)$, thus, become pure imaginary and real values, respectively. It is also observed that both the real part and imaginary part of $F(f, g)$ are on the same order of 10^{-3}, which confirms that the quadratic term $T_2(f, g)$ plays the same important role in the TCC approximation as the linear term $T_1(f, g)$ does, with a relatively large amount of individual Zernike aberration. Considering the individual aberration in current lithographic projection lens is typically less than 0.1λ, the TCC quadratic approximation will provide

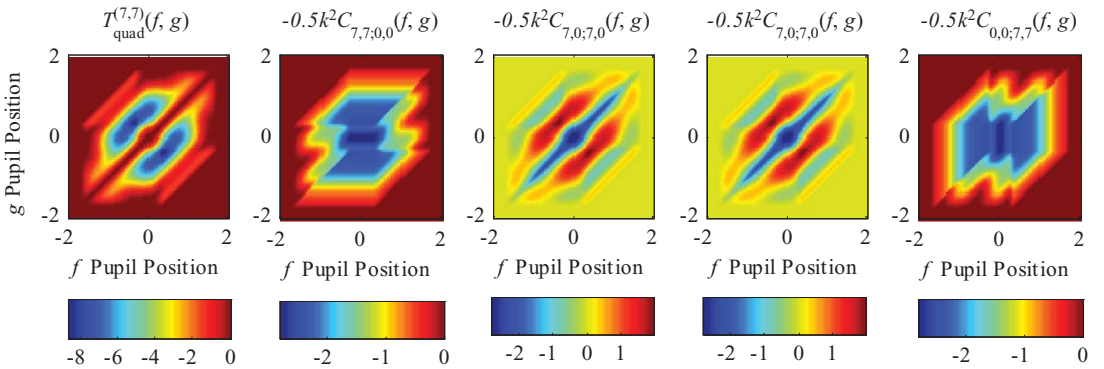

Fig. 7 Representation of the quadratically aberrated TCC term $T_{quad}^{(7,7)}(f, g)$ as a sum of weighted CTCs.

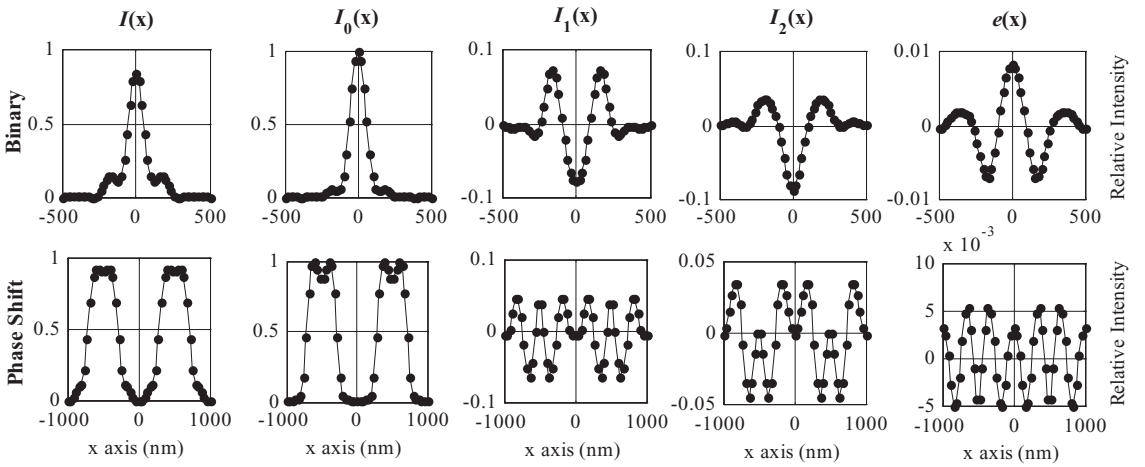

Fig. 8 Simulation results of the quadratic aberration model for the binary grating and alternating phase shift grating under the input parameters: NA = 0.75, λ = 193 nm, $Z_9 = 0.1\lambda$, σ = 0.35, and defocus = 100 nm.

an efficient approach in the TCC modeling with a high degree of accuracy.

Figure 6 illustrates the calculated CTCs for $T_{\text{lin}}^{(7)}(f, g)$, which multiplied by Z_7 is equal to the linear term $T_1(f, g)$ in Fig. 5. Figure 7 represents the CTCs for $T_{\text{quad}}^{(7,7)}(f, g)$, which multiplied by squared Z_7 is equal to the quadratic term $T_2(f, g)$ shown in Fig. 5. It is interesting to note that the pairs of CTCs, such as $[C_{7,0;0,0}(f, g), C_{0,0;7,0}(f, g)]$, $[C_{7,7;0,0}(f, g), C_{0,0;7,7}(f, g)]$, and $[C_{7,0;7,0}(f, g), C_{7,0;7,0}(f, g)]$ are exactly the same except the coordinates (f, g) are exchanged with each other. This is due to the mathematical property of CTCs as expected in Eq. (16). Therefore, for the purpose of fast calculation and simulation, we need to calculate only half of the CTCs to achieve the TCC quadratic approximation.

3.3 *Simulation of the Cross Triple Correlation-based Quadratic Aberration Model*

To simulate the CTC-based quadratic aberration model, we set the imaging system operating at λ = 193 nm and NA = 0.75 with a partial coherence factor of 0.35 and defocus of 100 nm. Both the one-dimensional binary grating (pitch = 1000 nm, opening width = 100 nm) and alternating phase shift grating (pitch = 1000 nm, opening width = 500 nm) were utilized as input mask patterns for example. The total image intensity can be decomposed and represented as a quadratic aberration model, which is expressed by the sum of the aberration-free intensity $I_0(\mathbf{x})$, linear intensity term $I_1(\mathbf{x})$, and quadratic intensity term $I_2(\mathbf{x})$. The error of the quadratic aberration model is introduced as $e(\mathbf{x})$ with the expression of $e(\mathbf{x}) = I(\mathbf{x}) - [I_0(\mathbf{x}) + I_1(\mathbf{x}) + I_2(\mathbf{x})]$.

Figure 8 shows the simulation results of the binary grating and alternating phase shift grating under the input of an individual Zernike coefficient $Z_9 = 0.1\lambda$, which is an even type aberration. From Fig. 8, it is noted that both the linear $I_1(x)$ and quadratic $I_2(x)$ terms contribute to a symmetrical effect on the image intensity distribution, as the aberration-free intensity $I_0(x)$ is symmetrical about $x = 0$. It is also observed that the model error $e(x)$ is as small as on the order of 10^{-3}, when the maximum value of $I_0(x)$ is normalized to 1.

Figure 9 illustrates the simulation results of the binary grating and alternating phase shift grating under the input of an individual Zernike coefficient $Z_7 = 0.1\lambda$, which is an odd type aberration. From Fig. 9, it is observed that the

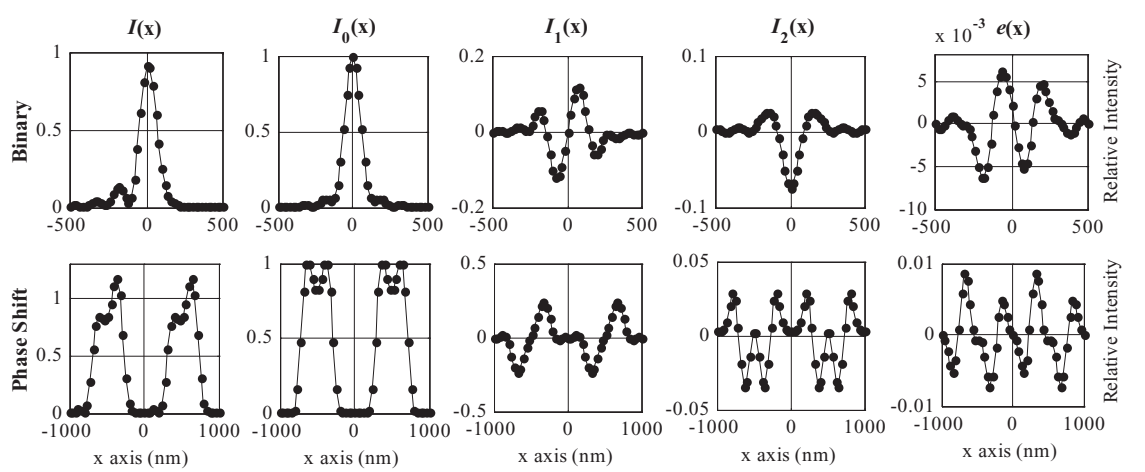

Fig. 9 Simulation results of the quadratic aberration model for the binary and alternating phase shift gratings under the input parameters: NA = 0.75, λ = 193 nm, $Z_7 = 0.1\lambda$, σ = 0.35, and defocus = 100 nm.

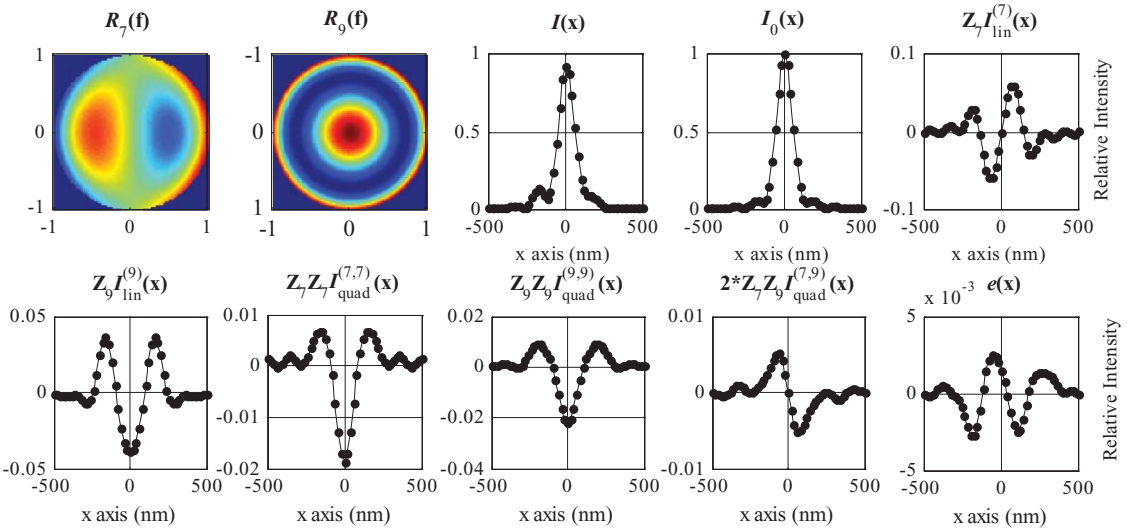

Fig. 10 Simulation results of the quadratic aberration model for the binary grating under the input parameters: NA = 0.75, $\lambda = 193$ nm, $Z_7 = 0.05\lambda$ and $Z_9 = 0.05\lambda$, $\sigma = 0.35$, and defocus = 100 nm.

linear term $I_1(x)$ shows an asymmetrical effect on the image intensity distribution, obviously different from that in Fig. 8. However, the quadratic term $I_2(x)$ in Fig. 9 depicts a symmetrical intensity distribution similar to that shown in Fig. 8. It is also noted that the model error $e(x)$ keeps a small value on the order of 10^{-3}, which demonstrates that the quadratic aberration model achieves a high accuracy in the aerial image intensity approximation.

The interaction of Z_7 and Z_9 on the aerial imaging was further simulated. Figure 10 shows the simulation result of the binary grating under the input individual Zernike coefficients $Z_7 = 0.05\lambda$ and $Z_9 = 0.05\lambda$. Comparing Fig. 10 to Figs. 8 and 9, it is noted that all the simulated terms in Fig. 10 can be classified into self-dependent terms and cross-interaction terms. For instance, the linear term $I_{lin}{}^{(7)}(x)$ and the quadratic term $I_{quad}{}^{(7,7)}(x)$ are called self-dependent terms as they are determined by the individual Zernike order Z_7, while the quadratic terms $I_{quad}{}^{(7,9)}(x)$ and $I_{quad}{}^{(9,7)}(x)$ are defined as cross-interaction terms as they are determined by interactions of two different Zernike orders Z_7 and Z_9. Due to the fact that $I_{quad}{}^{(7,9)}(x)$ and $I_{quad}{}^{(9,7)}(x)$ are equal, the $I_{quad}{}^{(7,9)}(x)$ can be simply doubled for the final simulation result, instead of taking into account the sum of $I_{quad}{}^{(7,9)}(x)$ and $I_{quad}{}^{(9,7)}(x)$.

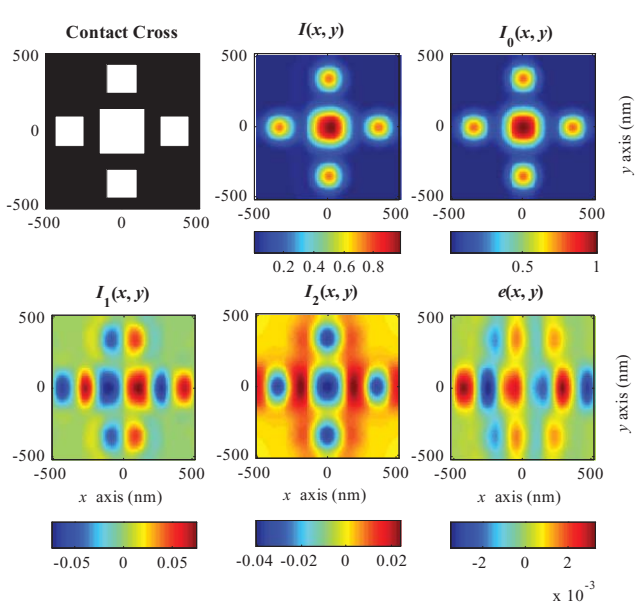

Fig. 11 Simulation results of the quadratic aberration model for the contact cross pattern under the input parameters: NA = 0.75, $\lambda = 193$ nm, $Z_7 = 0.1\lambda$, $\sigma = 0.70$, and defocus = 0 nm.

Except for the fact that one-dimensional masks with multiple pitches and orientations were input for simulations, a contact cross pattern was also designed as a two-dimensional mask for simulating the quadratic aerial image model. Figure 11 depicts the calculation results based on the contact cross pattern with setting parameters of NA = 0.75, $\lambda = 193$ nm, $Z_7 = 0.1\lambda$, $\sigma = 0.70$, and defocus = 0 nm. From Fig. 11, it is observed that the linear term $I_1(x, y)$ appears asymmetrical about x axis but symmetrical about y axis, while the aberration-free intensity $I_0(x, y)$ is symmetrical about $(x, y) = (0,0)$. This effect is due to the asymmetric property of Z_7 aberration about f axis on the pupil plane. The quadratic term $I_2(x, y)$ contributes a symmetric effect on the image intensity distribution, similar to the one-dimensional symmetric property of $I_2(x)$ shown in Fig. 11. The one-dimensional intensity distributions can be thus considered as a cross section ($y = 0$) of the two-dimensional intensity distributions. From this observation and lots of other simulation results for binary and phase shift masks with multiple pitches and orientations, it is found that the proposed CTC-based quadratic aberration model is suitable and efficient for one/two-dimensional aerial image approximation with a high degree of accuracy.

4 Conclusions

We propose a CTC-based method suitable for fast calculation and evaluation of a quadratic aberration model in partially coherent imaging systems. By further investigating the Hopkins' imaging theory, a TCC quadratic approximation is proposed for characterizing TCC up to the quadratically

aberrated term. A quadratic aberration model is subsequently established for aerial image calculation and decomposition, based on the TCC quadratic approximation. Each term in the TCC quadratic approximation can be represented as a weighted sum of several CTCs. Due to the fast algorithm for calculating CTCs, the TCC quadratic approximation and the quadratic aerial image model can be efficiently obtained. Simulations were performed by the proposed CTC-based algorithm with different input Zernike aberrations for binary and phase shift masks with multiple pitches and orientations, which demonstrate that the proposed approach is not only accurate but also efficient for revealing the influence of different Zernike orders on aerial image intensity distributions under partially coherent illumination. It is expected that this method will have direct applications in the aerial image-based aberration analysis and metrology. It will also have potential applications in the robust OPC and inverse mask design with aberrations taken into account.

Acknowledgments

This work was supported by National Natural Science Foundation of China (Grant Nos. 91023032 and 51005091) and Fundamental Research Funds for the Central Universities of China (Grant No. 2010ZD004). The authors would like to thank National Engineering Research Center for Lithographic Equipment of China for supporting this work.

References

1. B. W. Smith and R. Schlief, "Understanding lens aberration and influences to lithographic imaging," *Proc. SPIE* **4000**, 294–306 (2000).
2. W. Liu, S. Y. Liu, T. T. Zhou, and L. J. Wang, "Aerial image based technique for measurement of lens aberrations up to 37th Zernike coefficient in lithographic tools under partial coherent illumination," *Opt. Express* **17**, 19278–19291 (2009).
3. W. Liu, S. Y. Liu, T. L. Shi, and Z. R. Tang, "Generalized formulations for aerial image based lens aberration metrology in lithographic tools with arbitrarily shaped illumination sources," *Opt. Express* **18**, 20096–20104 (2010).
4. F. Zernike, "Beugungstheorie des Schneidenverfahrens und seiner verbesserten form, der Phasenkontrastmethode," *Physica (Amsterdam)* **1**, 689–704 (1934).
5. F. Wang, X. Z. Wang, and M. Y. Ma, "Measurement technique for in situ characterizing aberrations of projection optics in lithographic tools," *Appl. Opt.* **45**, 6086–6093 (2006).
6. B. Peng, X. Z. Wang, Z. C. Qiu, and Q. Y. Yuan, "Measurement technique for characterizing odd aberration of lithographic projection optics based on dipole illumination," *Opt. Commun.* **283**, 2309–2317 (2010).
7. Q. Y. Yuan, X. Z. Wang, Z. C. Qiu, F. Wang, and M. Y. Ma, "Even aberration measurement of lithographic projection system based on optimized phase-shifting marks," *Microelectron. Eng.* **86**, 78–82 (2009).
8. T. Nakashima, K. Higashi, and S. Hirukawa, "Impact of Zernike cross-term on linewidth control," *Proc. SPIE* **4691**, 33–43 (2002).
9. B. E. A. Saleh, "Optical bilinear transforms," *Opt. Acta* **26**, 777–799 (1979).
10. H. van der Laan, M. Dierichs, H. van Greevenbroek, E. McCoo, F. Stoffels, R. Pongers, and R. Willekers, "Aerial image measurement methods for fast aberration setup and illumination pupil verification," *Proc. SPIE* **4346**, 394–407 (2001).
11. D. G. Flagello, J. Klerk, G. Davies, and R. Rogoff, "Towards a comprehensive control of full-field image quality in optical photolithography," *Proc. SPIE* **3051**, 672–685 (1997).
12. T. Nakashima, S. D. Slonaker, T. Kudo, and S. Hirukawa, "Evaluation of Zernike sensitivity method for CD distribution," *Proc. SPIE* **5040**, 1600–1610 (2003).
13. A. R. Neureuther, L. Wang, M. Miller, E. Chin, C. Clifford, K. Yamazoe, N. Xu, and T. King-Liu, "Physics-based models for process awareness," presented at the *2010 Lithography Workshop*, Lihue, Kauai, USA, 7–11 November 2010.
14. L. Zavyalova, A. Bourov, and B. W. Smith, "Automated aberration extraction using phase wheel targets," *Proc. SPIE* **5754**, 1728–1737 (2005).
15. L. V. Zavyalova, B. W. Smith, A. Bourov, G. Zhang, V. Vellanki, P. Reynolds, and D. G. Flagello, "Practical approach to full-field wavefront aberration measurement using phase wheel targets," *Proc. SPIE* **6154**, 61540Y (2006).
16. H. H. Hopkins, "On the diffraction theory of optical images," *Proc. R. Soc. London, Ser. A* **217**, 408–432 (1953).
17. R. R. Shannon and J. C. Wyant, *Applied Optics and Optical Engineering*, Vol. XI Academic, New York (1992).
18. A. W. Lohmann and B. Wirnitzer, "Triple correlations," *Proc. IEEE* **72**, 889–901 (1984).
19. R. Köhle, "Fast TCC algorithm for the model building of high NA lithography simulation," *Proc. SPIE* **5754**, 918–929 (2005).
20. R. E. Crochiere and L. R. Rabiner, *Multirate Digital Signal Processing*, Prentice-Hall, Englewood Cliffs, NJ (1983).

Shiyuan Liu is a professor of mechanical engineering at Huazhong University of Science and Technology, leading his Nanoscale and Optical Metrology Group with research interest in the metrology and instrumentation for nanomanufacturing. He also actively works in the area of optical lithography, including partially coherent imaging theory, wavefront aberration metrology, optical proximity correction, source mask optimization, and inverse lithography technology. Professor Liu received his PhD in mechanical engineering from Huazhong University of Science and Technology in 1998. He is a member of SPIE, OSA, IEEE, and CSMNT (Chinese Society of Micro/Nano Technology). He holds 12 patents and has authored or co-authored more than 100 technical papers.

Wei Liu is currently a PhD candidate at Huazhong University of Science and Technology under the guidance of Professor Shiyuan Liu. He received his BS degree from the Physics School of the same university in 2007. His research involves various issues in optical lithography, including wavefront aberration metrology, and inverse lithography technology. He is a student member of SPIE.

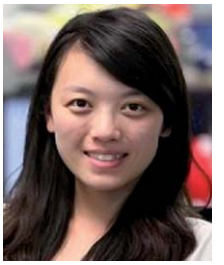

Tingting Zhou is a graduate student at Huazhong University of Sicence and Technology, pursuing her master degree in mechanical engineering under the guidance of Professor Shiyuan Liu. She received her BS degree from the Physics School of the same university in 2008. Her research interests include optical lithography simulation and fast aerial image calculation.